Statistics of the Air–Sea Fluxes of Momentum and Mechanical Energy in a Coupled Wave–Atmosphere Model

SUSANNE L. WEBER

Royal Netherlands Meteorological Institute, De Bilt, the Netherlands

(Manuscript received 28 May 1993, in final form 1 November 1993)

ABSTRACT

An atmospheric general circulation model (GCM) and a wind wave model are coupled through the wind stress. The wind stress, which forces the wave model, depends in the coupled model on the stage of development of the wave field. As the waves depend on the local and instantaneous wind as well as the earlier wind elsewhere, nonlocal and memory effects are thus introduced in the momentum flux parameterization. It is examined how strong these effects are compared to the local and instantaneous wind contribution. A second variable considered is the energy flux from the atmosphere to the wave field, which can be determined diagnostically from the wave model.

Almost all of the momentum and energy passed to the wave field is lost quasi-instantaneously and locally to the ocean, whereas only a small fraction remains in the local wave field or propagates away. The momentum and energy contained in the wave field are determined by the small difference between input and dissipation. This small difference depends strongly on the memory of the wave field. Wave propagation also influences the local balance. The case for the fluxes is different. A memory effect is only visible in the momentum flux for storms that last relatively long. In general, the typical time scale of wind changes is smaller than that of wave evolution. Nonlocal effects can be neglected in both the momentum flux and the energy flux. These results indicate that, at the present state of the art in wave and climate modeling, the wave effect on the air–sea fluxes can be described adequately in (coupled) atmosphere–ocean GCMs by the local and instantaneous wind.

1. Introduction

Wind waves are an obvious feature of the interface between atmosphere and ocean. Intuitively, one would expect the air–sea fluxes to be modified by their presence. Whether this is indeed the case has been the subject of extensive research; see Donelan (1990) for a thorough overview. Recent results on the dependence of the momentum and water vapor flux on the sea state are those obtained in the HEXOS field experiment (Maat et al. 1991; DeCosmo 1991; Smith et al. 1992). Theoretical models of the momentum flux were put forward by Janssen (1989, 1991) and by Chalikov and Makin (1991). Both theory and measurements indicate that the surface momentum flux is enhanced at the initial stage of wave development. The case for the latent and sensible heat fluxes is not clear.

Present atmospheric and oceanic general circulation models (AGCMs and OGCMs) do not take the sea state into account. The question arises if it is important to do so. Recently, Hasselmann (1991) proposed to couple the atmosphere and the ocean through an explicit model of their interface: surface gravity and capillary waves. As a first step Weber et al. (1993) coupled a climate AGCM (ECHAM; Roeckner et al. 1992) to a wave model (WAM; WAMDI Group 1988), using the coupling formalism of Janssen (1989, 1991). In the atmosphere–wave–ocean system the wave field is generated by and interacts with the atmospheric flow, whereas the ocean does not directly modify the surface waves. Therefore, it makes sense to first examine the atmosphere–wave subsystem.

Weber et al. concentrated on the impact of the wave field on the large-scale atmospheric flow. They found that in the coupled WAM–ECHAM the enhancement of the surface stress is too small to significantly modify the climatological mean circulation. This is consistent with results from an earlier pilot study (Ulbrich et al. 1993).

The coupled WAM–ECHAM model is the first model that computes the surface stress taking the wave effect into account. This creates the opportunity of studying, for the first time, the wave effect in a global dataset that extends over several months. The wave field has a memory much longer than the wind memory. Waves can propagate over large distances. The wave field at any particular time and location thus depends on the history and spatial structure of the wind field as well as on the local and instantaneous wind. Nonlocal and memory effects are therefore introduced in the stress formulation when the stress is computed taking the sea

Corresponding author address: Dr. Susanne L. Weber, Royal Netherlands Meteorological Institute, P.O. Box 201, 3730 AE, De Bilt, the Netherlands.

state into account. These effects are not there when the flux is derived from the atmospheric model alone. In the present analysis the nonlocal and memory effects, which are introduced by WAM, are compared to the local and instantaneous wind contribution.

Although the wave effect is too small to modify the large-scale atmospheric circulation, a different flux formulation might modify the coupled atmosphere–ocean system. A clear picture of the wave effect on the air–sea fluxes answers the question of whether wind waves have to be taken into account in coupled atmosphere–ocean GCMs.

The model of coupled wind–wave growth applied in WAM–ECHAM was verified against HEXOS field data for a number of idealized cases. The present study examines if it is also consistent with the HEXOS results in a realistic simulation. There are many approaches to modeling the wave effect on the air–sea fluxes (Donelan 1990). The aim of the present paper is not to assess the validity of this particular approach as a model of wind wave growth. It is simply adopted here as an (acceptable) model. The aim is rather to describe the impact of an explicit wave model on the surface stress and to examine if the wave effect can be parameterized in terms of atmospheric parameters. The latter is important because WAM takes fairly much computing time: in its present resolution, which is standard in the global version, it needs four times as much CPU as ECHAM.

The momentum flux is a prognostic variable of the atmospheric model. In the coupled wave–atmosphere model it depends on the sea state, which in turn depends on the wind stress. In coupled atmosphere–ocean models the ocean is forced by the wind stress. A second parameter considered in the analysis is the mechanical energy flux. It is a diagnostic variable, which can easily be derived from the wave model. The energy flux is a forcing term for ocean models with an explicit mixed layer.

The present analysis is performed on a three-month permanent-July simulation with the coupled WAM–ECHAM model. There is two-hourly output of instantaneous wave and wind parameters. In section 2 of this paper the fluxes of momentum and energy from the atmosphere to the waves and from the waves to the ocean are defined. In section 3 the total air–sea momentum flux and its sea state dependence is discussed. The areas of significant wind–wave interaction in the coupled WAM–ECHAM simulation are identified in section 4. The momentum flux is analyzed in section 5. The total air–sea energy flux and its modification by the wave field is described in section 6 and analyzed in section 7. Shortcomings of the models used are discussed in section 8. A summary of the results is given in section 9. The data used are described in the Appendix.

2. The wave momentum and wave mechanical energy

The wave field is commonly described in terms of the variance spectrum F of the surface elevation. Here $F = F(\omega, \theta; \mathbf{x}, t)$, where ω is the radian frequency and θ the propagation direction of a wave component; $\mathbf{x}$ denotes the space coordinate and t is time. The evolution equation for the spectrum is (cf. WAMDI Group 1988):

$$\frac{\partial F}{\partial t} + \mathbf{c}_g \cdot \frac{\partial F}{\partial \mathbf{x}} = S_{\text{in}} - S_{\text{dis}} + S_{\text{nl}}. \tag{1}$$

On the left-hand side are the local time derivative and advection by wave propagation with the group velocity $\mathbf{c}_g$. The right-hand side contains the so-called source terms: wind input S_{in}, dissipation by whitecapping S_{dis} and the redistribution of wave variance by resonant four-wave interactions S_{nl}. This last term is known from first principles. The interactions conserve variance, energy, and momentum. Therefore this term disappears after integration over the frequency-direction domain. The net effect of the resonant interactions is to shift the energy-containing range of the spectrum to lower frequencies. The other two source terms are not so well known, but there is agreement in the wave community on their basic features.

The wind input was computed numerically by Janssen (1989) from the quasi-stationary boundary-layer equations. As boundary conditions he used the wind speed at the top of the boundary layer and the surface spectrum. The growth rate and the total surface stress were found to depend on the stage of development of the wave field. An efficient approximation to this model (Janssen 1991) is used in WAM to compute S_{in} and to couple WAM to the atmospheric model.

The total wave momentum $\mathbf{P}$ and energy E follow from the variance spectrum as

$$\mathbf{P} = \rho_0 \left\langle \omega \frac{\mathbf{k}}{k} F \right\rangle \quad \text{and} \quad E = \rho_0 \left\langle \frac{\omega^2}{k} F \right\rangle. \tag{2}$$

Here the angle brackets denote integration over the frequency-direction domain, ρ_0 is the density of ocean water, and k is the modulus of the wavenumber $\mathbf{k}$. The momentum and energy fluxes to and from the wave field are found from (1) and (2) as (Komen 1987):

$$\tau_{\text{aw}} = \left.\frac{\partial \mathbf{P}}{\partial t}\right|_{\text{wind}} = \rho_0 \left\langle \omega \frac{\mathbf{k}}{k} S_{\text{in}} \right\rangle, \tag{3}$$

$$\tau_{\text{wo}} = \left.\frac{\partial \mathbf{P}}{\partial t}\right|_{\text{whitecaps}} = \rho_0 \left\langle \omega \frac{\mathbf{k}}{k} S_{\text{dis}} \right\rangle, \tag{4}$$

$$\epsilon_{\text{aw}} = \left.\frac{\partial E}{\partial t}\right|_{\text{wind}} = \rho_0 \left\langle \frac{\omega^2}{k} S_{\text{in}} \right\rangle, \tag{5}$$

$$\epsilon_{\text{wo}} = \left.\frac{\partial E}{\partial t}\right|_{\text{whitecaps}} = \rho_0 \left\langle \frac{\omega^2}{k} S_{\text{dis}} \right\rangle. \tag{6}$$

The subscript aw denotes a flux from the atmosphere to the wave field and the subscript wo denotes a flux from the wave field to the ocean. The magnitude of the momentum fluxes will be denoted by τ_{aw} and τ_{wo}.

The definitions (3)–(6) suggest that the fluxes can be computed directly from the wave model. This is not quite true as the integrals extend over all frequencies, whereas WAM computes (1) only up to a given cutoff frequency (WAMDI Group 1988). This is partly for reasons of computational efficiency and partly because the high-frequency behavior of the individual source terms is badly known. For the high-frequency range, equilibrium between the sources and sinks is assumed and the spectral form is prescribed. A second complication is that the dissipation term S_{dis} is formally divergent for frequencies tending to infinity.

The momentum flux τ_{aw} is computed as follows. The low-frequency contribution is found by integration of (3) up to the cutoff frequency and the high-frequency contribution is parameterized (Janssen 1991). The energy flux ϵ_{aw} is approximated by representing the phase velocity $c = \omega/k$ in (5) by its mean value over the frequency range. This yields:

$$\epsilon_{aw} = c\tau_{aw}, \tag{7}$$

where c is the mean phase velocity. The fluxes τ_{wo} and ϵ_{wo} from the wave field to the ocean are estimated from the total wave momentum and energy budgets. Integrating (1) over the frequency–direction domain yields to a good approximation:

$$\tau_{wo} = \tau_{aw} - \frac{\partial P}{\partial t} - \mathbf{c}_g \cdot \frac{\partial P}{\partial \mathbf{x}}, \tag{8}$$

where P is the modulus of the wave momentum $\mathbf{P}$. A similar equation can be derived for the wave energy E. The momentum and energy budgets will be evaluated in sections 5 and 7. In the following the terms on the right-hand side of (8) are denoted by *wind input, local growth/decay,* and *advection.*

In the discrete coupling scheme the atmospheric model ECHAM communicates the wind friction velocity u_* (defined in section 3) to the wave model at the end of every time step (40 min). WAM then performs the same time step. Integral wave parameters are computed from the wave spectrum and written on tape every 2 h. This yields time series of the two-dimensional field of u_* and the corresponding fields of the wave variance, mean propagation direction, mean frequency, and wave-induced stress. All other wave parameters considered in the analysis are derived from these fields (see the Appendix).

3. The surface momentum flux in the WAM–ECHAM model

In the present model the atmospheric loss of momentum at the air–sea interface is thought to consist of two parts. One related to turbulence in the atmospheric boundary layer and the other related to the random wave field (Janssen 1989, 1991). The latter is defined in (3). Note that not all of the momentum lost to the waves is available to the ocean as a part remains in the local wave field and a part propagates away, possibly dissipating later or elsewhere. However, this is irrelevant from the atmospheric point of view.

In the following the surface stress will be denoted by τ_{ao}. It is parameterized as

$$\tau_{ao}/\rho_a = u_*^2 = c_D U^2, \tag{9}$$

with ρ_a the air density, u_* the friction velocity, U the wind speed at a reference height, and c_D the drag coefficient. Under neutral conditions c_D depends on the surface roughness z_0 only. Here z_0 is modeled by the Charnock (1955) relation:

$$z_0 = \alpha u_*^2/g, \tag{10}$$

where g is the gravitational constant. In the coupled WAM–ECHAM model $\alpha = \alpha_C$, where α_C depends on the wave field (Janssen 1989, 1991),

$$\alpha_C = \frac{\beta}{(1 - \tau_{aw}/\tau_{ao})^n}, \tag{11}$$

with $n = 0.8$. The proportionality constant β is chosen so that $\alpha_C = 0.018$ for saturated waves, that is, waves in equilibrium with the wind. This is a mean value (Wu 1980), which is used in the standard ECHAM without the wave model coupled to it. Equations (9)–(11) implicitly define τ_{ao} and α_C as functions of the instantaneous local wind U and the wave stress τ_{aw}. The latter depends on the instantaneous local wind as well as the earlier two-dimensional wind field because of memory effects and wave propagation.

Simultaneous measurements of wind and wave parameters in the HEXOS field experiment have resulted in an empirical expression $\alpha = \alpha_H$ (Maat et al. 1991; Smith et al. 1992):

$$\alpha_H = \mu A_p^{-1}, \tag{12}$$

where $\mu = 0.5$ and the wave age is defined as $A_p = c_p/u_*$, with c_p the phase velocity corresponding to the peak of the wind sea spectrum (Smith et al. 1992). In the HEXOS analysis only actively generated, undersaturated waves were considered, with $10 < A_p < 30$. This excludes wave fields with a significant swell component, that is, oversaturated waves, which generally have been generated by storms elsewhere. Furthermore, only single-peaked spectra were taken into account. The expression (11) was validated against HEXOS data for the restricted class of spectra considered in the HEXOS analysis (Janssen 1992).

In the coupled model all kinds of spectra can occur. In section 5 I will compare the (prognostically used) α_C with a (diagnostically determined) modified form of (12):

$$\alpha'_H = \mu A^{-1}, \qquad (12')$$

with $A = c/u_*$. As c is an integral quantity it is straightforward to compute for all spectra. For the HEXOS cases c is about 10% smaller than c_p, but it has the same evolution.

Let us compute some simple cases of wave evolution under homogeneous conditions. When the wind is constant the spectrum evolves in such a way that the total energy increases and the energy-containing range of the spectrum shifts to lower frequencies, until equilibrium is reached. As lower frequencies correspond to higher phase velocities, the wave age increases during wave evolution. At the initial stage of wave development one finds a stress ratio $R = \tau_{aw}/\tau_{ao}$ of about 0.9 and a wave age $A = c/u_*$ of about 10. They tend rapidly to their equilibrium value ($R \sim 0.55$ and $A \sim 28$) as more and more wave components become saturated. From (11) and (12') it follows that at the initial stage of growth α_C and α'_H have about three times their equilibrium value.

When there is a strong increase in wind speed R is found to increase and A to decrease, quasi-instantaneously. This is followed by gradual relaxation to equilibrium. When the wind drops a large number of low-frequency wave components becomes oversaturated. The presence of swell results in a value of R below its equilibrium, whereas the value of A is above its equilibrium. The situation of a turning wind is comparable to an increase in wind speed, but the effect is less pronounced. In the following a field with $R > 0.55$ will be denoted as *undersaturated,* whereas a wave field with $R < 0.55$ will be denoted as *oversaturated.*

4. Areas of significant wind–wave interaction

The areas of significant wind–wave interaction are indicated in Fig. 1, which gives the frequency of occurrence of undersaturated waves ($R > 0.55$). In the Arabian Sea and in the Southern Hemisphere storm track undersaturated waves occur 20%–40% of the time. Everywhere else, apart from some isolated spots, this is less than 10% of the time. The Indian monsoon is at its peak in July and strong surface winds occur in the Arabian Sea, giving rise to intense wave generation. In the storm track fetch-limited effects are clearly visible in the maximum off the South American continent. These seem to be interesting areas, but they are not well represented in the present coarse resolution. Therefore they are not considered in the following. The maximum of 40% in the frequency of occurrence of undersaturated waves coincides with a maximum in storm intensity. The winds are relatively strong and variable in this area. The mean wind friction velocity shows a pattern very similar to Fig. 1, with a maximum mean u_* of 40 cm s^{-1}. The analysis will be restricted to the open sea in the Southern Hemisphere storm track, with emphasis on the area where the interaction between the waves and the atmospheric flow is strongest.

In the storm track the time-mean stress ratio R is about 0.3, whereas the time mean over cases of undersaturated waves only is about 0.65. In the area of maximum wind–wave interaction, $R > 0.65$ occurs typically 20% of the time, whereas $R > 0.75$ is found only 1% of the time. The wave age A can also be used as a measure of wind–wave interaction. The frequency of occurrence of young waves ($A < 28$) is only 25% in the area of maximum storm intensity. Lower wave ages occur typically less frequent than the corresponding stress ratios. The reason for this will become clear in section 5 by looking in more detail at the stress ratio and the wave age.

In the following sections the wave effect will be illustrated by an example time series at a randomly cho-

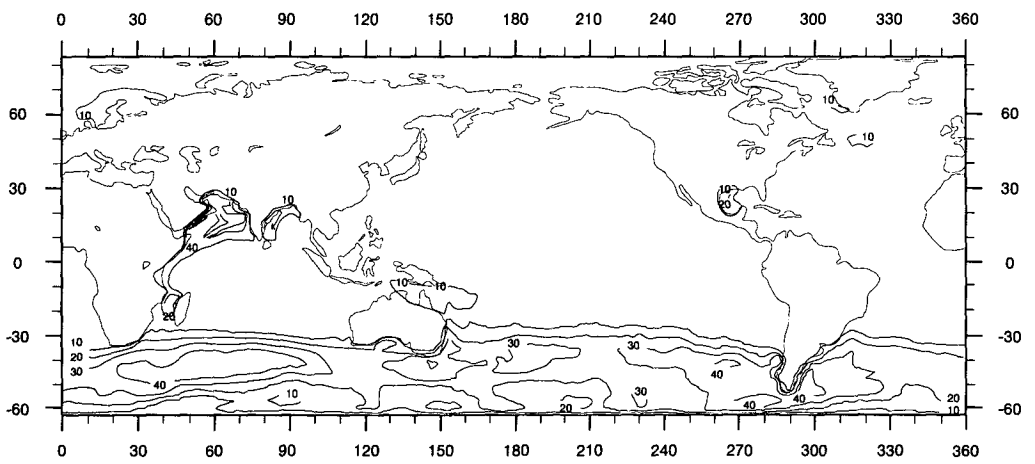

FIG. 1. Percentage of time that the ratio R of momentum input into the wave field to the total air–sea momentum flux is larger than 0.55 in a 3-month permanent-July experiment with the coupled WAM–ECHAM model. The value $R = 0.55$ occurs when wind and waves are in equilibrium and no swell is present.

sen location (42°S, 27°E) in the area of maximum frequency of occurrence of undersaturated waves. All parameters studied show similar behavior at other locations in this area.

5. Statistics of the momentum flux

First the integral momentum budget (8) is considered. Figure 2 gives a time series of the total air–sea flux τ_{ao}, the flux to the wave field τ_{aw}, the local growth/decay term and the advection term. In the storm track the last two terms have approximately the same magnitude. This indicates that the *momentum contained in the wave field* is determined by local processes as well as wave propagation. The growth/decay term and the advection term are 10%–20% of the wind input on average. From (8) it thus follows that τ_{wo} differs by ±20%–40% from τ_{aw} on average. However, taking only cases of undersaturated waves into account, the relative importance of the terms in the momentum budget becomes different. Now local growth/decay is typically 2%–4% of the wind input and advection is typically 1%–3% of the input. About 95% of the momentum gained by undersaturated waves is thus passed on quasi-instantaneously and locally to the ocean. Only 5% remains in the local wave field or propagates away, possibly dissipating later or elsewhere. These figures are consistent with the JONSWAP estimates (Hasselmann et al. 1973). In the cases of interest here, namely, undersaturated wave fields, one can, to a good approximation, set $\tau_{wo} = \tau_{aw}$.

The correlation between τ_{aw} and τ_{ao} is larger than 0.9 everywhere in the storm track. This shows that *the momentum flux through the wave field* is strongly determined by the local wind. A representation of the wave stress by a constant times the wind stress is a very good approximation. However, the small misfit in this representation is exactly the variable part of the wave effect, which is of interest. The wave effect is given by α_C, see (11). As a first step to analyze α_C, a comparison is made between α_C and the empirical variable α'_H, see (12′). Figure 3 shows a time series of α_C and α'_H. The two parameters are normalized in the figure with the equilibrium value $\alpha = 0.018$, so that values larger than one correspond to cases of undersaturated waves ($R > 0.55$ in α_C) or young waves ($A < 28$ in α'_H).

There is pronounced variability in α_C at the output period of 2 h, occurring mainly in the case of undersaturation. Presumably this high-frequency variability is due to changes in the details of the spectral shape, especially at the short wave components. Then there is variability in α_C at periods of 1–3 days. At these longer periods α_C agrees well with α'_H, although α'_H tends to be somewhat lower. Undersaturated (oversaturated) waves coincide largely with young (old) waves. The agreement between α_C and α'_H is not systematically better for young wind sea than for old waves. Note that α_C can be larger than one for small

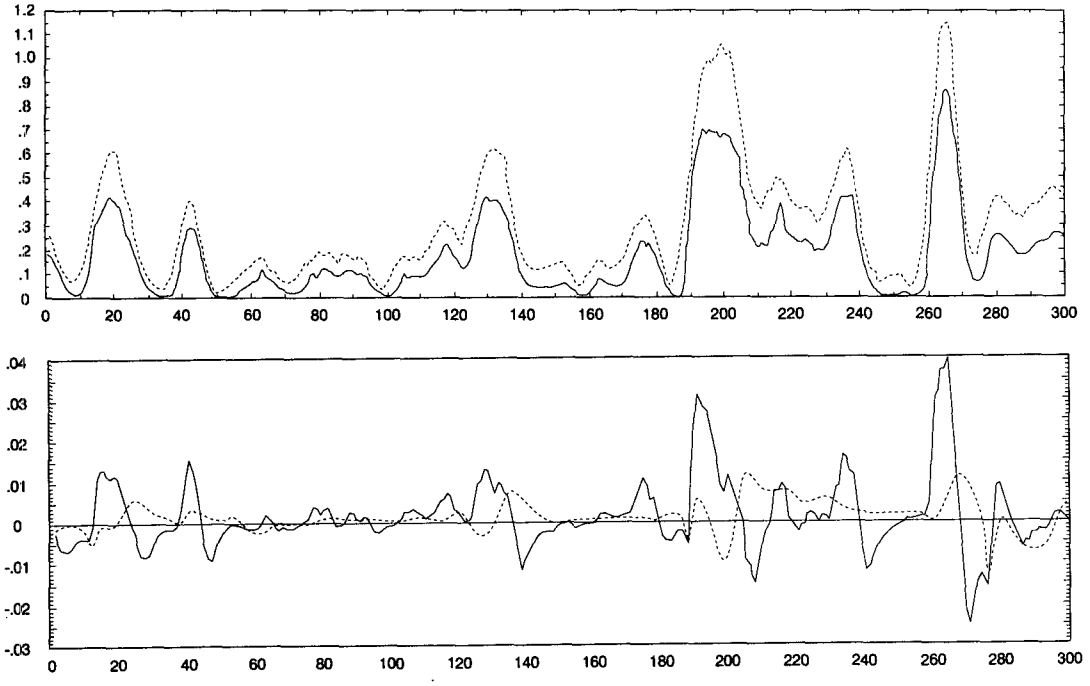

FIG. 2. (a) The momentum input into the wave field (solid line) and the total air–sea momentum flux (dashed line), in units of kg $(s^3\ m)^{-1}$. (b) The local wave growth/decay (solid line) and advection of wave momentum (dashed line), in units of kg $(s^3\ m)^{-1}$. Time series over 25 days from the coupled WAM–ECHAM permanent-July experiment, with time in units of the output interval of 2 h. Location is 42°S, 27°E.

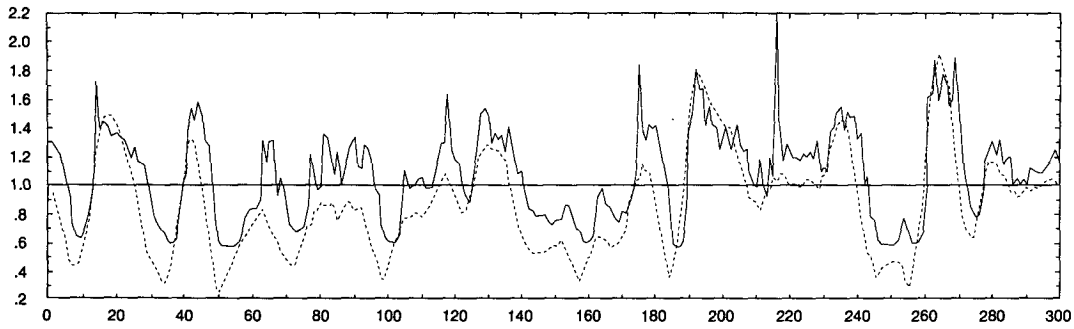

FIG. 3. The Charnock parameter as computed from the coupled wind-wave model $\alpha_C = 0.01/(1 - R)^{0.8}$ (solid line) and as computed from the modified HEXOS relation $\alpha'_H = 0.5/A$ (dashed line), where R is the stress ratio and A is the wave age. Both parameters are scaled with the equilibrium value $\alpha = 0.018$, so that values larger than 1 indicate cases of undersaturated ($R > 0.55$) or young ($A < 28$) waves. Data as in Fig. 2.

local growth or even decay (cf. Fig. 2b). In these cases high-frequency wave components actively grow, although the dominant part of the spectrum shows little growth or even decay. The variable α'_H is more consistent with the local wave evolution. Variability in α'_H can be due only to shifts of the dominant part of the spectrum over the frequency range (or to changes in the wind stress). It is not clear to what extent the peaks in α_C, which are absent in the corresponding time series of α'_H, are realistic.

To investigate the separate contribution of wind changes and wave evolution to the variability in α'_H, time series of u_*/c and u_* are compared in Fig. 4a. Here u_* is scaled with a representative value for the wave phase velocity. The typical sea state is represented by $c = 14$ m s^{-1}, which corresponds to a typical wavelength of 120 m and typical wave periods of 8 sec. This holds for the entire storm track in the WAM–ECHAM simulation. The equilibrium value $A = c/u_* = 28$ is indicated in the figure. It is clear that the variability in the inverse wave age is fairly well given by the wind information alone. There is only one storm (time units 190–210) where the wave field ages before the wind weakens.

Figure 4b gives a time series of the mean phase velocity c, normalized with the representative value of 14 m s^{-1}. The location and the time period are the same as for the time series shown earlier. Cases of undersaturated waves, which can be identified from Fig. 3, are indicated in Fig. 4b. The time series shows that for undersaturated waves c tends to first decrease and then to increase gradually. This can be explained as follows. As the wind strengthens the dominant part of the spectrum first shifts from low-frequency swell to undersaturated, actively growing wind sea. Then, due to internal wave dynamics, the energy containing part of the wind sea spectrum gradually moves to lower frequencies. Only during the storm at the end of the time period (time units 190–210) is the change in c so large that the wave evolution contributes significantly to the variability in the inverse wave age. Just after this storm (units 210–230) the advection of low-frequency wave components (cf. Fig. 2b) is reflected in a decrease in mean phase velocity. This is the only event with a systematic mismatch between u_*/c and $u_*/14$. In all other cases the wind determines the wave age, as the wave response to the wind field is slow compared to the time scale of wind changes. Note that in HEXOS the variability in the wave phase velocity was also found to be much smaller than the variability in the wind friction velocity (Smith et al. 1992).

The parameter α'_H can be approximated by $\tilde{\alpha}_H = u_*/28$, as $A^{-1} \sim u_*/14$. Now compare α_C with $\tilde{\alpha}_H$ (Fig. 5). It is clear that at periods of 1–3 days the agreement between α_C and $\tilde{\alpha}_H$ has deteriorated in some cases and improved in others in comparison to α'_H (Fig. 3). A cross-spectral analysis (Fig. 6) shows that α_C and u_* have a correlation of 0.6–0.8 at periods of 1–3 days, where u_* leads with about 6 hours at periods of 1 day and has zero lead at longer periods. The variance spectrum of α_C is an order of magnitude larger than that of u_* at short periods, but has equal magnitude at periods larger than one day. The correlation (over all periods) between α_C and u_* is typically 0.7–0.8 in the entire storm track.

One can conclude that α_C exhibits variability at periods of hours and at periods of 1–3 days. The former is not visible in α'_H. Therefore it is not clear how realistic this feature is. This high-frequency variability can be attributed to changes in the details of the spectral shape and might be a model artifact. Variability at periods of 1–3 days, which seems realistic, is also found in α'_H. Both in α_C and α'_H this low-frequency variability is mainly determined by the wind, but in part also by the development of the wind sea spectrum during a storm. The duration of a storm, not its strength, seems to determine if this effect is visible. Nonlocal effects on the wave age are very weak. The wave effect on the atmospheric loss of momentum, as given by α_C, is thus well represented by u_*. For undersaturated waves almost all of the momentum input is passed on quasi-instantaneously and locally to the ocean. Therefore,

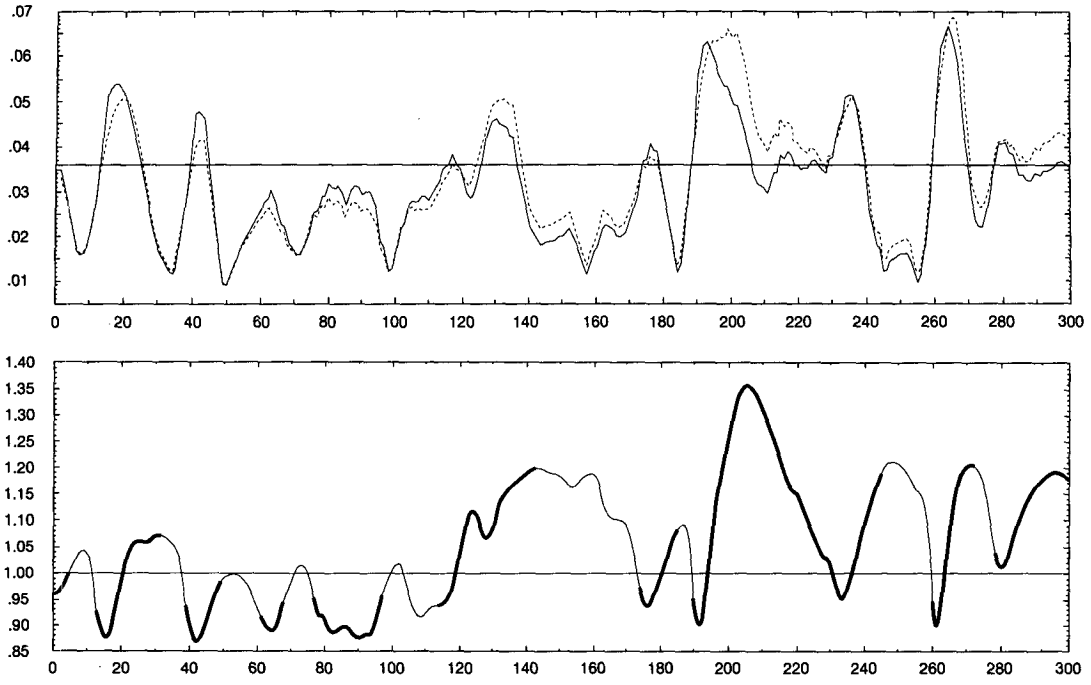

FIG. 4. (a) The inverse wave age $A^{-1} = u_*/c$ (solid line) and the wind friction velocity u_*. The latter is scaled with a typical value of the wave phase velocity of 14 m s^{-1} (dashed line). (b) The wave phase velocity c, scaled with a typical value of 14 m s^{-1}. Solid segments denote cases of undersaturated waves (cf. Fig. 3). Data as in Fig. 2.

the wave effect on the oceanic gain of momentum can equally well be represented by the local and instantaneous wind alone.

6. The surface energy flux in the WAM–ECHAM model

Airflow over the ocean surface generates turbulent kinetic energy (TKE) in the oceanic upper boundary layer. This can be by turbulent shear stresses on the surface, shear flow production by wind-driven currents in the oceanic boundary layer, or by generation and subsequent breaking of surface waves. All these processes are denoted by "wind stirring." They are important when there is a strong wind generating intense wave motion. Actively growing waves exhibit strong breaking, which is then probably the dominant source of wind-generated TKE.

A tentative description of the combined turbulent and wave motion in the oceanic boundary layer is given by Kitaigorodskii and Lumley (1983), who discuss possible mechanisms for the transformation of wave mechanical energy into TKE. Applying this framework to field data, Kitaigorodskii et al. (1983) propose a two-layer structure for the oceanic boundary layer. It consists of an upper layer, characterized by intense

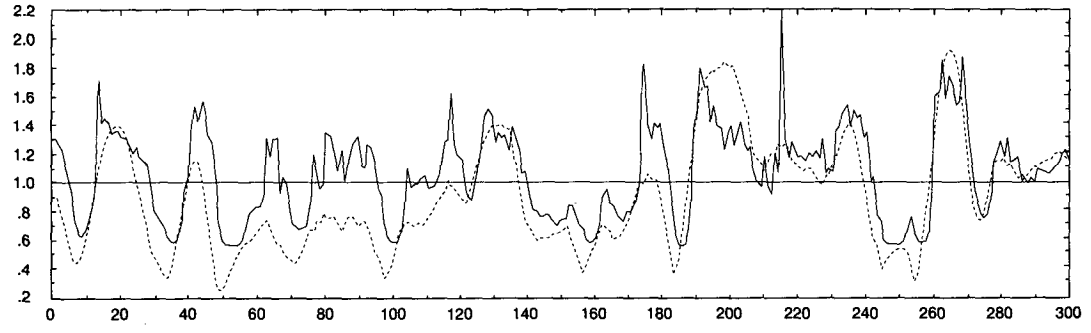

FIG. 5. The Charnock parameter as computed from the coupled wind-wave model $\alpha_C = 0.01/(1 - R)^{0.8}$ (solid line) and as approximated by $\tilde{\alpha}_H = u_*/28$ (dashed line), where R is the stress ratio. Both parameters are scaled with the equilibrium value $\alpha = 0.018$. Data as in Fig. 2.

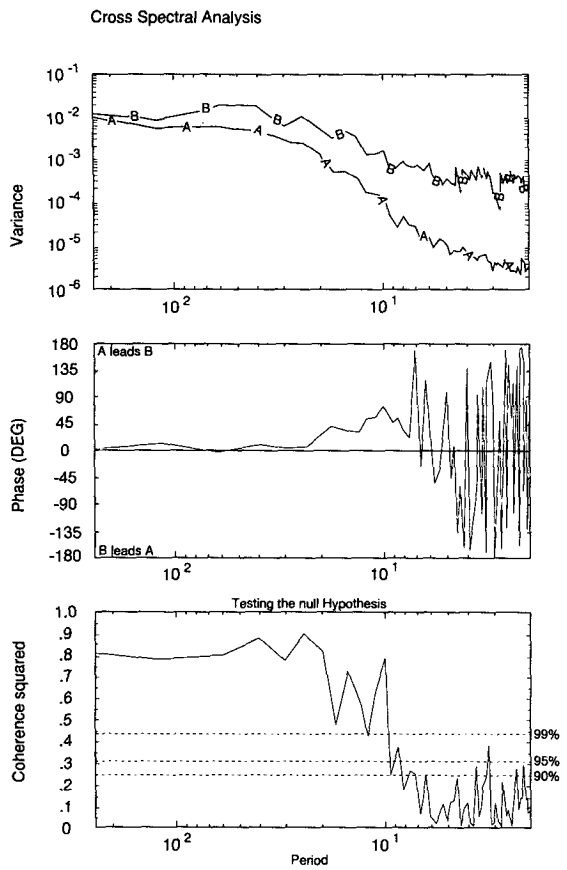

FIG. 6. Variance spectra, phase lead and coherence squared of the Charnock parameter as computed from the coupled wind-wave model $\alpha_C = 0.01/(1 - R)^{0.8}$ (denoted as B) and the wind friction velocity u_* (denoted as A). Data used are 9 chunks of 10 days at 42°S, 27°E, time unit is 2 h.

wave-induced turbulence, and a lower, constant stress layer. The latter is expected when waves are not present.

These results do not yield a dissipation expression that can be applied in a wave model nor a source term that can be applied in a mixed layer model. The present treatment of the wave effect on the energy flux is therefore much cruder than that of the momentum flux. I will simply compare the energy flux obtained from WAM with a standard mixed layer approach. The energy input into the wave field is given by (7) as $\epsilon_{aw} = c\,\tau_{aw}$. Wind stirring, that is, the rate of working by the wind on the water, is commonly parameterized as

$$\epsilon_{ao} = m\rho_a u_*^3, \tag{13}$$

where m is a proportionality factor of order one (Niiler and Kraus 1977).

The penetration depth of wind-generated TKE scales with the Ekman depth λ_E (Wells 1979), given by

$$\lambda_E = w_*/f, \tag{14}$$

where $w_* = (\rho_a/\rho_0)^{1/2} u_*$ is the friction velocity in the *oceanic* boundary layer and f the Coriolis parameter. In the case of wave-generated TKE a different length scale should be applied. Huang (1986) proposes, on the basis of theoretical concepts of wave breaking, the dominant wavelength. This is also indicated by the data of Kitaigorodskii et al. (1983). The mean wavelength L, which characterizes the depth of the wave orbital motions, is used here.

7. Statistics of the energy flux

Consideration of the energy budget gives results similar to the case of the momentum budget. About 95% of the energy gained by undersaturated waves in the storm track is lost to the ocean. It is therefore justified to set $\epsilon_{wo} = \epsilon_{aw}$. The flux to the wave field ϵ_{aw} is well correlated with the total air–sea flux ϵ_{ao}. In the storm track the correlation is everywhere larger than 0.95.

A remarkable feature of the WAM dissipation term is that it yields values for ϵ_{aw} typically one order of magnitude larger than u_*^3. In Fig. 7a time series of ϵ_{ao} and ϵ_{aw} are shown. The proportionality factor in (13) is set $m = 14$, so that the two quantities have (in the mean) equal magnitude. The energy flux ratio $\epsilon_{aw}/\epsilon_{ao} = AR/14$ is given in Fig. 7b. Cases of undersaturated waves, which can be identified from Fig. 3, are indicated in the figure. The energy flux ratio shows variability comparable to the variability in the momentum flux ratio τ_{aw}/τ_{ao}. However, for undersaturated waves the energy flux ratio tends to be fairly constant. This is not surprising, as the wave age A and the stress ratio R are anticorrelated at periods of 1–3 days (see section 5). The product AR is therefore rather insensitive to the stage of development of the wave field. It is about 14 everywhere in the storm track. The energy flux through the wave field shows the same functional dependence on the wind friction velocity as one would expect from the conventional parameterization.

The mean Ekman depth λ_E shows a pattern similar to that of the frequency of occurrence of young waves (see Fig. 1) in the storm track. It is 150 m in the area of maximum storm intensity in the Indian Ocean, decreasing to 100 m at the edges of the storm track. The mean wavelength L is 120 m in the storm track, with lower values of 80 m directly west of the South American continent where the waves are typically less developed. The differences between the mean length scales seem negligible. The wavelength is less variable than the Ekman depth. (This can be inferred from Fig. 4a, which gives a time series of u_* and $c \sim \sqrt{L}$.) The depth of the wave orbital motions is thus fairly constant.

The large value of the parameter m obtained from WAM can indicate several things. First, the dissipation in the wave model might simply be too strong. This is discussed further in section 8. Second, the air–sea en-

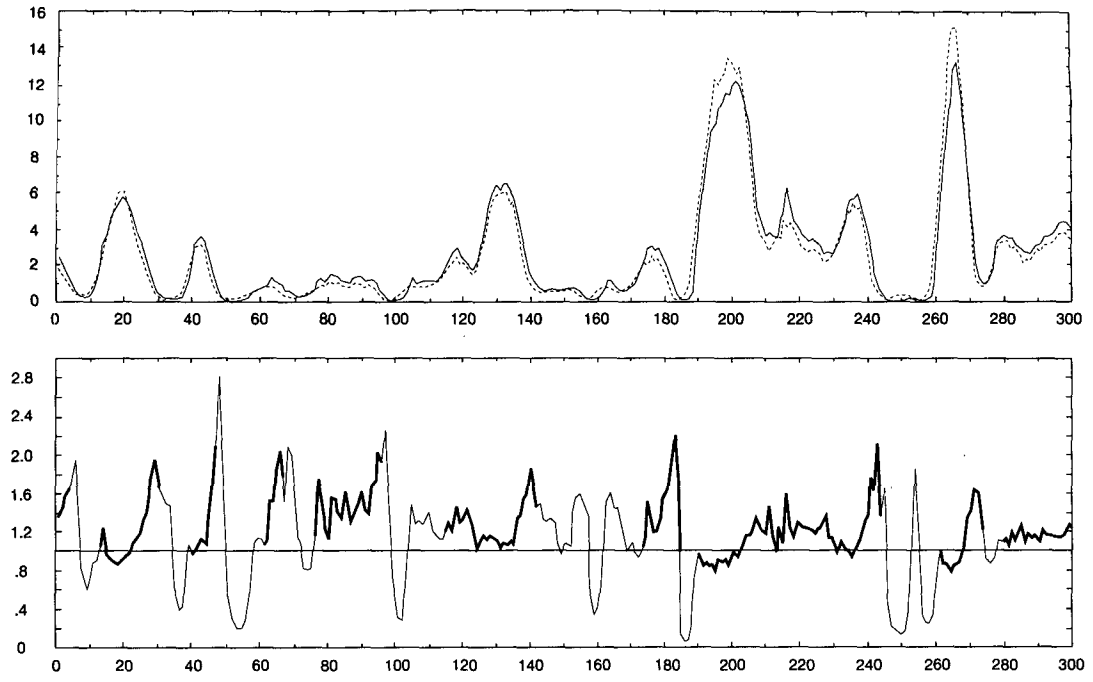

FIG. 7. (a) The energy flux from the atmosphere to the wave field $\epsilon_{aw} = ARu_*^3$ (solid line) and the total air–sea energy flux $\epsilon_{ao} = m\,u_*^3$ (dashed line), in units of $m^3\,s^{-3}$, with $m = 14$. (b) The ratio $AR/14$ of the wave energy flux ϵ_{aw} to the total energy flux ϵ_{ao}. Solid segments denote cases of undersaturated waves, compare Fig. 3. Data as in Fig. 2.

ergy flux might be much larger than is commonly assumed. Huang (1986) gives an overview of proposed values for m, which range from 0 to 50. The present value is within this range. It might be realistic in the case of undersaturated waves. It is not clear how deep TKE generated by breaking waves can penetrate into the oceanic boundary layer. The mean wavelength obtained from WAM suggests that the zone of wave influence is as deep as the Ekman depth on average. However, at present theoretical and experimental knowledge on wave–turbulence interaction is still incomplete. It is therefore not possible to draw any definite conclusion.

8. Discussion

Computation of the air–sea fluxes through the wave field is a new application of WAM. It is important to realize that the model has been tuned and verified for other purposes, that is, predicting the wave spectrum. Diagnostic variables like the total wave energy and the mean wave frequency, which are mainly determined by the low-frequency part of the spectrum, have been validated extensively. This implies that the sum of the source terms is rather well known. However, the individual source terms determine the fluxes. Both S_{in} and S_{dis} contain empirical constants. Different values than the ones presently used in WAM can as well yield the desired net input (Burgers and Makin 1993). Moreover, the high-frequency behavior of the wind input and the dissipation term is badly known.

The momentum flux through the wave field is sensitive to the high-frequency spectral range. The stress ratio R thus depends on an uncertain feature of WAM. In section 5 it was shown that R behaves similar to the inverse wave age, which depends on the well verified mean phase velocity. The energy flux through the wave field was computed as $\epsilon_{aw} = c\tau_{aw}$. It seems therefore justified to assume that τ_{aw} and ϵ_{aw} are qualitatively well described by WAM. However, their value might be overestimated. Burgers and Makin (1993) show that the input and dissipation term can be chosen four to five times smaller than in the standard WAM. Clearly this would yield lower values for the fluxes through the wave field.

The occurrence of extreme events is restricted in the present coupled model for a number of reasons. First, the high-frequency range is not explicitly computed in WAM. Suppose, for example, that α_C and α'_H are about five times their equilibrium value ($R \sim 0.95$ and $A \sim 5$). A wave age $A \sim 5$ corresponds to a mean radian frequency of 1.3 Hz when $u_* \sim 1.5\ m\ s^{-1}$. The mean frequency is higher when u_* is lower. A spectrum centered around 1.3 Hz can be resolved in the present model, but for higher mean frequencies one would have to extend the standard frequency range. This would increase the CPU and memory demands considerably.

Second, the present spatial resolution of 3° × 3°, which corresponds to a minimum fetch of 300 km in the storm track, cannot resolve fetch-limited growth. This would be of interest off coasts and in enclosed basins, where the stage of development of the wave field depends on the fetch. This is already visible in the present model (see Fig. 1), but it would become much more pronounced at a resolution of about 50 km. Over open sea the WAM resolution seems to be adequate, as the spatial scale of the resolved atmospheric flow is much larger anyway.

Thirdly, extreme wind events are rare at the present resolution of the atmospheric model (about 5.6° × 5.6°). Going to higher resolution AGCMs show more intense storm activity and fronts can be resolved. However, the results from section 5 indicate that not the strength but the duration of a storm determines how strongly α_C depends on the local and instantaneous wind. Therefore, with stronger surface winds α_C would be more enhanced, but it would still be highly dependent on u_*. Increasing the WAM resolution as well as the ECHAM resolution would yield more spatial structure in the stress ratio field. Extending finally the frequency range as well, high stress ratios could occur for weak winds. This seems to be the least relevant aspect of the coupled model resolution, as the time scale for growth to saturation is very short for weak winds. Summarizing: at higher spatial resolution the interaction between waves and the atmospheric flow might become stronger, both due to higher stress ratios and increased spatial inhomogeneity. However, it seems likely that the dependence of the fluxes through the wave field on the local and instantaneous wind would remain strong.

9. Conclusions

Theoretically the wave model introduces nonlocal and memory effects in the flux formulation. In the present simulation nonlocal effects are negligible. For the wave momentum flux τ_{aw} memory effects are only visible when the surface winds remain strong for a relatively long time. Then the wave field can grow to saturation before the wind weakens. In general the wave evolution is too slow compared to the typical time scale of wind changes. For the wave energy flux $\epsilon_{aw} = c\tau_{aw}$ memory effects are absent, because there are two compensating processes. As waves evolve, the mean wave phase velocity c increases whereas the wave stress τ_{aw} decreases. Taking the cpu demands of WAM and the accuracy of other parameterizations in ECHAM into account, one can conclude that the wave effect on the surface fluxes is adequately represented by the local and instantaneous wind. If this is done, the total surface momentum flux depends on a roughness length, which scales with u_*^3. In the standard parameterization this is u_*^2. The wave age can be estimated from u_*. The total surface energy flux scales with u_*^3 as is the standard approach.

The wave momentum and energy budgets are determined by local growth/decay, an advection term, input by the atmospheric flow and dissipation by whitecapping. It was found that the first two terms are small for undersaturated waves. About 95% of the atmospheric input into the developing wave field is passed on quasi-instantaneously and locally to the ocean. The present results therefore apply to the wave–ocean fluxes as well as to the atmosphere–wave fluxes. At this point it is important to make a clear distinction between the *momentum and energy fluxes through the wave field* and the *momentum and energy contained in the wave field.* The wave momentum and energy are determined strongly by nonlocal and memory effects. A full wave model is needed in order to predict these parameters. The fluxes through the wave field, on the other hand, depend mainly on local and instantaneous processes. They can be parameterized in terms of one atmospheric parameter, the wind friction velocity. This is also the standard approach. The present results show why this standard approach works, although the wave field itself is a very complex system.

The coupled WAM–ECHAM model has a coarse resolution of about 5.6° × 5.6°. Extreme events are therefore rare. Moreover, the computation of the fluxes through the wave field is a new application of WAM. It is not clear how well the fluxes are modeled, especially their dependence on the high-frequency tail of the spectrum. Keeping these reserves in mind, the present study should be considered as a first assessment of the wave effect on the air–sea fluxes. The analysis shows that the wave effect can be well approximated using the wind information alone. The case for much higher-resolution wave and atmosphere models, combined with improved knowledge of the short wave components, remains to be investigated.

Acknowledgments. I would like to thank Gerrit Burgers for discussions, Klaus Hasselmann for critically reading the manuscript, and Hans von Storch for his continuous support. Much of this work was done during various short visits to the Max-Planck-Institut für Meteorologie in Hamburg, Germany. Part of this research was funded by FC (EVSV-CT92-0125).

APPENDIX

Computation of Wave Parameters

The wave model WAM computes the evolution equation (1) on a regular 3° × 3° grid, forced by the wind friction velocity u_*. There is 2-hourly output (every three time steps) of instantaneous values of u_* and the corresponding total wave variance $\langle F \rangle$, mean radian frequency $\bar{\omega}$, mean propagation direction $\bar{\theta}$, and wave-induced stress τ_{aw}. The other parameters used in the analysis are derived from these in the following manner.

(i) *The phase velocity, group velocity, and wavelength.* From the dispersion relation $\omega^2 = gk$, it follows

that the phase velocity $c = \omega/k$, the group velocity $\mathbf{c}_g = \partial\omega/\partial k$, and the wavelength $L = 2\pi g/\omega^2$. The mean values c, $\mathbf{c}_g$, and L can be derived in a similar way, to a very good approximation, from $\bar{\omega}$.

(ii) *The approximate evolution equations for E and P.* Substituting the dispersion relation in the definition (2) it follows that the total wave energy E is given by

$$E = \rho_0 g \langle F \rangle. \tag{A1}$$

Integrating (1) over ω and θ and multiplying with a factor $\rho_0 g$ one obtains

$$\frac{\partial E}{\partial t} + \mathbf{c}_g \cdot \frac{\partial E}{\partial \mathbf{x}} = \epsilon_{aw} - \epsilon_{wo}. \tag{A2}$$

Here the group velocity in the advection term has been approximated by the velocity of the dominant part of the spectrum, which is represented by $\bar{\omega}$ and $\bar{\theta}$. A similar equation follows easily for the total wave momentum $\mathbf{P}$. Obviously this derivation neglects the effect of the (varying) spectral shape on the propagation term. These evolution equations are therefore only used to estimate the order of magnitude of the local growth/decay and advection term in comparison to the fluxes to and from the wave field. The wave evolution itself is computed in WAM from the full equation (1). Given the unknowns in the computation of the fluxes by the wave model (see section 8) these approximations seem to be acceptable.

REFERENCES

Burgers, G., and V. K. Makin, 1993: Boundary-layer model results for wind-sea growth. *J. Phys. Oceanogr.*, **23,** 372–385.

Chalikov, D. V., and V. K. Makin, 1991: Models of the wave boundary layer. *Bound.-Layer Meteor.*, **56,** 83–99.

Charnock, H., 1955: Wind stress on a water surface. *Quart. J. Roy. Meteor. Soc.*, **81,** 639–640.

DeCosmo, J., 1991: Air–sea exchange of momentum, heat and water vapor over whitecap sea states. Ph.D. thesis, University of Washington, 212 pp.

Donelan, M. A., 1990: Air–sea interaction. *The Sea,* Vol. 9A, B. LeMehaute and D. M. Ilanes, Eds., Interscience, 239–292.

Hasselmann, K., 1991: Ocean circulation and climate change. *Tellus,* **43**AB, 82–103.

——, T. P. Barnett, E. Bouws, H. Carlson, D. E. Cartwright, K. Enke, J. A. Ewing, H. Gienapp, D. E. Hasselmann, P. Kruseman, A. Meerburg, P. Muller, D. J. Olbers, K. Richter, W. Sell, and H. Walden, 1973: Measurements of wind-wave growth and swell decay during the Joint North Sea Wave Project (JONSWAP). *Dtsch. Hydrogr. Z.*, **12,** 95 pp.

Huang, N. E., 1986: An estimate of the influence of breaking waves on the dynamics of the upper ocean. *Wave Dynamics and Radio Probing of the Ocean Surface,* O. M. Philips and K. Hasselmann, Eds., Plenum, 295–313.

Janssen, P. A. E. M., 1989: Wave-induced stress and the drag of air flow over sea waves. *J. Phys. Oceanogr.*, **19,** 745–754.

——, 1991: Quasi-linear theory of wind generation applied to wave forecasting. *J. Phys. Oceanogr.*, **21,** 1631–1642.

——, 1992: Experimental evidence of the effect of surface waves on the airflow. *J. Phys. Oceanogr.*, **22,** 1600–1604.

Kitaigorodskii, S. A., and J. L. Lumley, 1983: Wave–turbulence interactions in the upper ocean. Part 1: The energy balance of the interacting fields of surface wind waves and wind-induced three-dimensional turbulence. *J. Phys. Oceanogr.*, **13,** 1977–1987.

——, M. A. Donelan, J. L. Lumley, and E. A. Terray, 1983: Wave-turbulence interactions in the upper ocean. Part II: Statistical characteristics of wave and turbulent components of the random vorticity field in the marine surface layer. *J. Phys. Oceanogr.*, **13,** 1988–1999.

Komen, G. J., 1987: Energy and momentum fluxes through the sea surface. *Dynamics of the Ocean Surface Mixed Layer,* P. Müller and D. Henderson, Eds., Hawai Institute of Geophysics Special Publications, 207–217.

Maat, N., C. Kraan, and W. A. Oost, 1991: The roughness of wind waves. *Bound.-Layer Meteor.*, **54,** 89–103.

Niiler, P. P., and E. B. Kraus, 1977: One-dimensional models of the upper ocean. *Modelling and Prediction of the Upper Layers of the Ocean,* E. B. Kraus, Ed., Pergamon, 143–177.

Roeckner, E., K. Arpe, L. Bengtsson, S. Brinkop, L. Dümenil, M. Esch, E. Kirk, F. Lunkeit, M. Ponater, B. Rockel, R. Sausen, U. Schlese, S. Schubert, and M. Windelband, 1992: Simulation of the present-day climate with the ECHAM model: Impact of model physics and resolution. Max-Planck-Institut für Meteorologie Report 93.

Smith, S. D., R. J. Anderson, W. A. Oost, C. Kraan, N. Maat, J. DeCosmo, K. B. Katsaros, K. L. Davidson, K. Bumke, L. Hasse, and H. M. Chadwick, 1992: Sea surface wind stress and drag coefficients: The HEXOS results. Bound.-Layer Meteor., **60,** 109–142.

Ulbrich, U., G. Bürger, D. Schriever, H. von Storch, S. L. Weber, and G. Schmitz, 1993: The effect of a regional increase in ocean surface roughness on the tropospheric circulation, a GCM experiment. *Climate Dyn.*, **8,** 277–285.

WAMDI Group, 1988: The WAM Model—a third generation ocean wave prediction model. *J. Phys. Oceanogr.*, **18,** 1775–1810.

Weber, S. L., H. von Storch, P. Viterbo, and L. Zambresky, 1993: Coupling an ocean wave model to an atmospheric general circulation model. *Climate Dyn.*, **9,** 63–69.

Wells, N. C., 1979: A coupled ocean atmosphere experiment—the ocean response. *Quart. J. Roy. Meteor. Soc.*, **105,** 355–370.

Wu, J., 1980: Wind stress coefficients over sea surface near neutral conditions. A revisit. *J. Phys. Oceanogr.*, **10,** 727–740.